

Water acceleration in a supraglacial channel predicts locations of step-pool sequence formation

Andreas ALEXANDER,^{1,2} Jeffrey A. TUHTAN,³ Maarja KRUUSMAA,^{3,4}
Thomas V. SCHULER,^{1,5} Andreas KÄÄB¹

¹*Department of Geosciences, University of Oslo, 0316 Oslo, Norway*

²*Department of Arctic Geology, The University Centre in Svalbard, 9171 Longyearbyen, Norway*

³*Centre for Biorobotics, Tallinn University of Technology, 12618 Tallinn, Estonia*

⁴*Centre for Autonomous Marine Operations and Systems, Norwegian University of Science and
Technology, 7491 Trondheim, Norway*

⁵*Department of Arctic Geophysics, The University Centre in Svalbard, 9171 Longyearbyen, Norway*

Correspondence: Andreas Alexander <andreas.alexander@geo.uio.no>

ABSTRACT. Supraglacial channels constitute an important part of the glacial hydrological system, both by influencing surface energy exchange as well as routing meltwater to eventually feed en- and subglacial drainage systems. Subglacial systems have received considerable scientific interest, but specific studies of supraglacial channels are sparse. This limited scientific understanding represents a missing link between meltwater generation and en/subglacial hydraulics; among others it poses a problem for constraining and validating glacier hydrological models. In this study, we utilize drifters carrying a navigation system to obtain the spatial and temporal evolution of the water velocity along a supraglacial channel on Austre Brøggerbreen (Svalbard). This velocity is then used to compute melt rates of the channel walls and to estimate the discharge in the channel. We further present, to our knowledge, the first dataset of the spatio-temporal evolution of the water acceleration in the channel. The highest accelerations occur at the location of step-pool

26 **sequences and peaks in the acceleration signal can already be seen before the**
27 **step-pool sequences have developed in the channel. We therefore conclude that**
28 **water acceleration can be used to predict where step-pool sequences will form.**

29 INTRODUCTION

30 Supraglacial streams and rivers play an important role in the transport of meltwater and energy along
31 the surfaces of glaciers and ice sheets. They also deliver meltwater into moulins, feed en- and subglacial
32 systems and thus influence glacier sliding at the ice base (e.g. Rippin and others, 2015; Gleason and others,
33 2016; Smith and others, 2017; Decaux and others, 2019; Pitcher and Smith, 2019) by changing the ice-bed
34 coupling (Iken and Bindshadler, 1986; Boulton and Hindmarsh, 1987; Mair and others, 2002). Surface
35 water reaching the glacier bed has been shown to influence its thermal regime (Alexander and others,
36 2020b). Cryo-hydrologic warming (Phillips and others, 2010, 2013) from refreezing surface meltwater is
37 further discussed in connection with large scale glacier instabilities (Dunse and others, 2015; Willis and
38 others, 2018). Surface water is not only transported into subsurface hydrological systems, but also routed
39 along the surface to downstream ecosystems (e.g. Nienow and others, 2017). Given the obvious importance
40 of supraglacial channels, it comes as a surprise that our knowledge of these highly dynamic systems is still
41 limited.

42

43 The cross-section of supraglacial channels ranges from a few centimeters to tens of meters in depth and
44 width (Germain and Moorman, 2016). Channels transport meltwater to the glacier margins, into moulins
45 or supraglacial lakes (Germain and Moorman, 2016). The appearance of supraglacial channels is primarily
46 controlled by surface topography (Yang and others, 2016) and their planform morphology is influenced by
47 the relationship between the channel incision and overall ice ablation rates (Jarosch and Gudmundsson,
48 2012; Karlstrom and others, 2013). The channel planforms are observed to develop meanders, thereby
49 enhancing heat production and heat transfer to the surrounding ice at bend apexes (Karlstrom and others,
50 2013) with the energy dissipation inside the channel being controlled by the surface melt (Mantelli and
51 others, 2015). The incision rates of channels into the ice depend on the water velocity as well as water
52 temperature (Isenko and others, 2005). Higher discharges or steeper slopes lead to faster incision and
53 higher sinuosity (Germain and Moorman, 2019), as higher discharge is accommodated by increased velocity
54 and steeper water surface slopes lead to higher velocities (Gleason and others, 2016). Recent work by

55 Germain and Moorman (2016) suggests, that the development of step-pool sequences and hence pulsating
56 flow is linked to the helical flow around the meander bends and not to high discharge as previously thought.
57

58 Pitcher and Smith (2019) identified in situ monitoring of supraglacial streams and rivers as a research
59 frontier to validate climate-based meltwater runoff models and ultimately improve the estimates of future
60 eustatic sea level changes. They further highlight that more field observations of channel incision rates
61 are needed to calibrate incision models (Pitcher and Smith, 2019) and thus project the formation and
62 evolution of supra- and englacial channels (e.g. Jarosch and Gudmundsson, 2012), as well as subglacial
63 systems (e.g. Gulley and others, 2009).

64

65 Most recent studies of the supraglacial system employ remote sensing to focus on the Greenland Ice
66 Sheet (GrIS) (e.g. Legleiter and others, 2014; Smith and others, 2015; Yang and others, 2015, 2016).
67 Satellite based water velocity measurements of rivers have, however, so far only been shown for ice covered
68 rivers during break-up of the ice cover (Kääb and others, 2019). A few studies focusing on local hydraulics
69 of supraglacial channels have been undertaken in recent years (e.g. Gleason and others, 2016; Germain and
70 Moorman, 2016, 2019). Gleason and others (2016) present detailed hydraulic measurements of the GrIS.
71 Their measurements are, however, limited to manual measurements at selected investigation sites. Full
72 understanding of the supraglacial system requires measuring the spatial distribution of flow parameters
73 over the whole flow path instead of only at selected sites.

74

75 In Alexander and others (2020a), we presented a drifter platform, which is able to log acceleration
76 data along the flow path of a supraglacial channel and estimate the velocity by integrating the
77 acceleration measurements. We also presented the acceleration distribution along a supraglacial channel.
78 Our measurements had, however, the disadvantage of lacking spatial reference. Linking the channel
79 morphology to the velocity and acceleration fields proved therefore difficult. Here we overcome this
80 challenge with a new global navigation satellite systems (GNSS) enabled drifter platform. By integrating
81 a GNSS receiver into our drifter we are able to not only measure accelerations, but also directly
82 receive information about position and displacement. We used this platform to conduct repeated field
83 measurements over an approximately 500 m long supraglacial channel section on Austre Brøggerbreen
84 (Svalbard) and present the spatial and temporal distribution of continuous acceleration and velocity

85 records along the channel. Here, we define the term “water acceleration” as the spatial and temporal
86 average of repeated field measurements of the surface water motion using the satellite positioning
87 drifters. We further use our measurements to calculate spatial and temporal variations of ice wall melt
88 along the channel and utilize Markov Chain - Monte Carlo (MCMC) analysis to estimate the channel
89 discharge. Finally, we use this dataset to compare it with the morphological evolution of the channel and
90 show how water acceleration can be used to predict the formation of step-pool sequences along the channel.
91

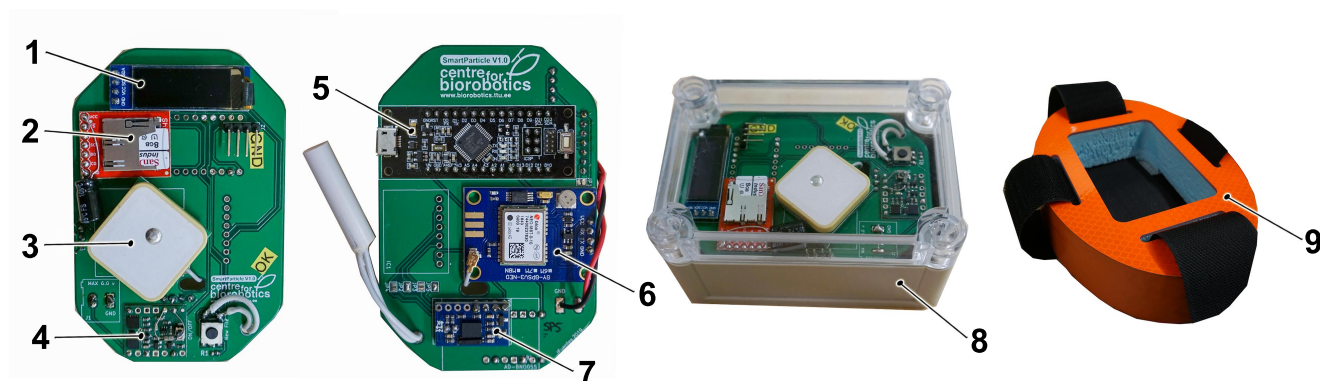
92 METHODS

93 Surface drifters

94 The 0.35 kg multimodal drifter (fig. 1) is buoyant and consists of a 0.25 m diameter foam floater disk
95 surrounding a waterproof box. This box houses two rechargeable lithium batteries (type 18650, 3.7 V,
96 3600 mA h) to power a custom-built printed circuit board, hosting a Bosch BNO055 inertial measurement
97 unit (IMU) and a NEO-M8T GNSS receiver. The latter records the x, y, z locations (EPSG: 4326, static
98 positioning accuracy of ± 3 m in x and y, ± 10 m in z) as well as the drifter velocity. The IMU measures
99 three components of the acceleration vector (m s^{-2}), magnetic field intensity (mT) and rate of rotation
100 ($^{\circ} \text{s}^{-1}$). Static positioning accuracy of the GNSS was estimated by comparing the static positions of the
101 individual drifters at the study site as they laid side-by-side over 15 minutes. Data were logged to a 8 GB
102 microSD card at a sampling rate of 5 Hz and stored as a delimited text file.

103 Field site and deployments

104 The Svalbard archipelago is located between 74° and 80°N and between 10° and 35°E . The annual air
105 temperature was -5.9°C between 1971 and 2000 with 196 mm annual precipitation in the same time
106 period at Svalbard airport (central Svalbard) (Hanssen-Bauer and others, 2019). About 59% of the land
107 surface is covered by glaciers (Nuth and others, 2013). The study glacier Austre-Brøggerbreen ($78^{\circ}54'\text{N}$,
108 $11^{\circ}49'\text{E}$) is a small, approximately 6 km^2 glacier located on a north facing slope of the Brøgger Peninsula
109 close to the research settlement Ny-Ålesund (fig. 2). The glacier extends from roughly 80 to 600 m above
110 sea level (a.s.l.) and has been rapidly down-wasting over the last years (Pope and others, 2007; Barrand
111 and others, 2010). The glacier has a network of several deeply incised supraglacial channels (e.g. Hagen and
112 others, 1991). The studied supraglacial stream occupies a persistent channel located on the northeastern



**1: LCD screen 2: microSD module 3: GNSS antenna 4: Power controller
5: Microcontroller 6: u-blox m8T (GNSS module) 7: IMU 8: IP68-cover
9: Buoyant floater**

Fig. 1. The surface drifter measurement device: a) Front side of the custom-built PCB, including LCD screen, SD storage, GNSS antenna and power controller. b) Back side of the PCB with microcontroller, GNSS module and IMU. c) Waterproof housing with transparent top cover. d) Foam floater disk with blank space to contain the drifter housing.

113 side of the glacier.

114

115 At the start of the fieldwork on 30.06.2019 the channel was still mainly snow covered and three step-pool
116 sequences visible. At the end of the fieldwork on 04.07.2019, the channel was completely snow free and
117 about 500 meters long with six clearly developed step-pool sequences in the lower part. We manually
118 deployed the drifters on three different days (30.06 with a deployment number $n=23$, 02.07 with $n=26$,
119 04.07 with $n=13$), dropping them into the channel at the highest possible location where the water
120 velocities were high enough to already transport the drifters (see fig. 2c and 3a,b). The drifter transects
121 became therefore longer each day as the snow melted and the channel developed. To recover the drifters, a
122 marine fishing net was temporarily installed at the end of the channel (black square in figure 2 and figure
123 3c), a few meters upstream of a 2 m high drop at the junction with a lateral channel. Two HOBO water
124 level loggers were installed during the fieldwork: The first (U20-001-02, Onset Computer Corp., USA) was
125 installed behind the recovery net in front of the drop (installed on the evening of the 30th of June) and
126 the second (U20L-02, Onset Computer Corp., USA) was installed further downstream at the outlet of an
127 englacial channel (brown circle in fig. 2c). The raw pressure accuracy was $\pm 0.3\%$ FS with a maximum

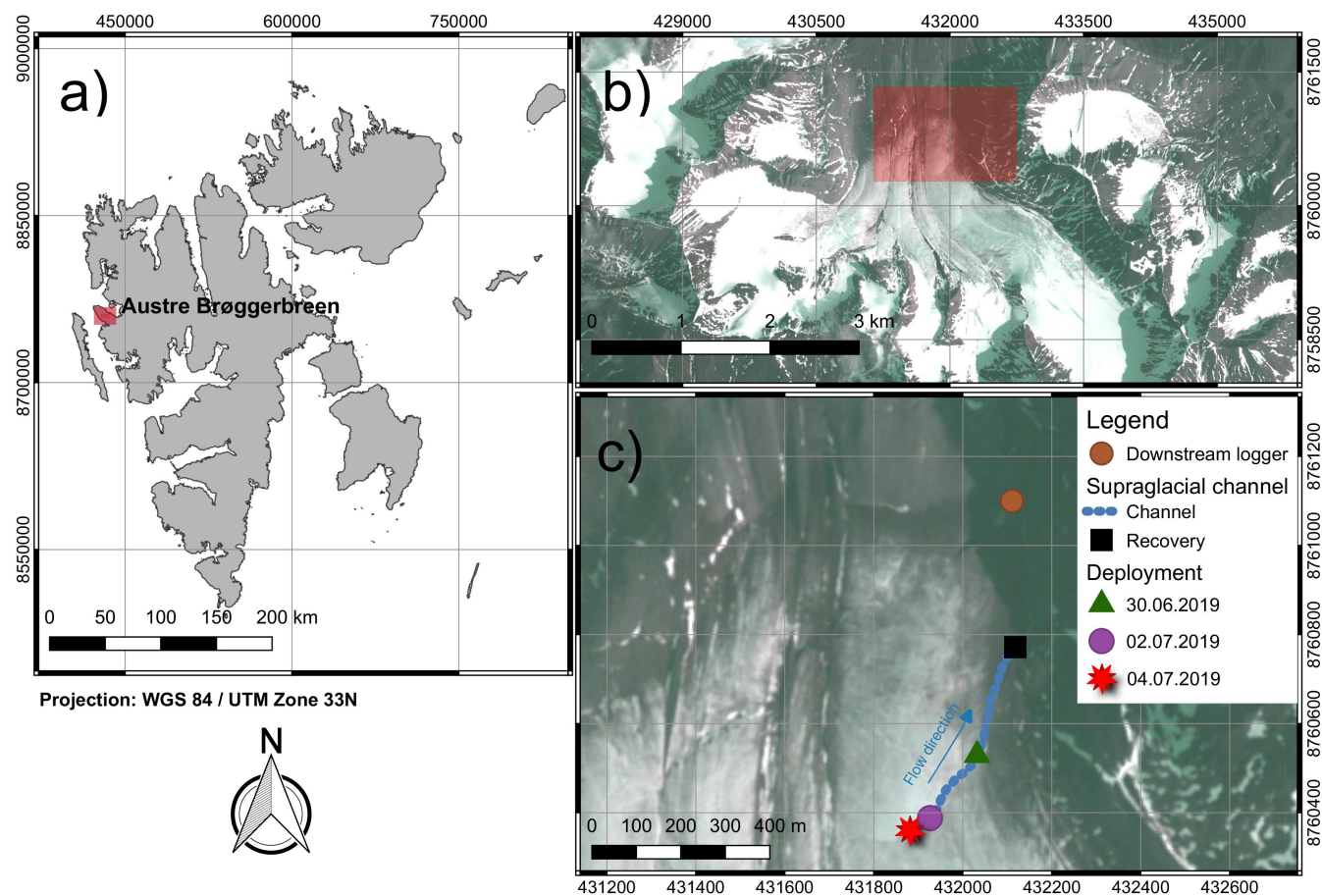


Fig. 2. The location of the study site on the Svalbard archipelago. b) Location of the supraglacial channel on Austre Brøggerbreen. c) The studied supraglacial channel with deployment points on the different field days (green triangle, purple circle, red star), recovery point (black square) and indicated flow direction. Further shown is the location of a second water level logger further downstream (brown circle). Background images: Planet scope from 09.07.2019 (Team Planet, 2017).

128 error of 1.20 kPa. Both loggers had a rated temperature accuracy of $\pm 0.44^{\circ}\text{C}$ from 0°C to 50°C , and a
129 drift of $0.1^{\circ}\text{C a}^{-1}$.

130

131 We used MATLAB R2018B to process all data. The data were filtered for outliers in an initial step,
132 based on the horizontal position accuracy of the GNSS signals (filter criteria: $> 3\text{ m}$ horizontal position
133 accuracy). Afterwards, additional outliers, which were more than 5 m away from the main track, were
134 removed manually and the offset of the timestamp was cut to obtain time after deployment. The coordinates
135 were then transformed into a Cartesian system (ETRS89 UTM 33 north). In a next step the x- and y-
136 coordinates were downsampled to a 2 m spacing using Gaussian scale space (Behrens and others, 2018).

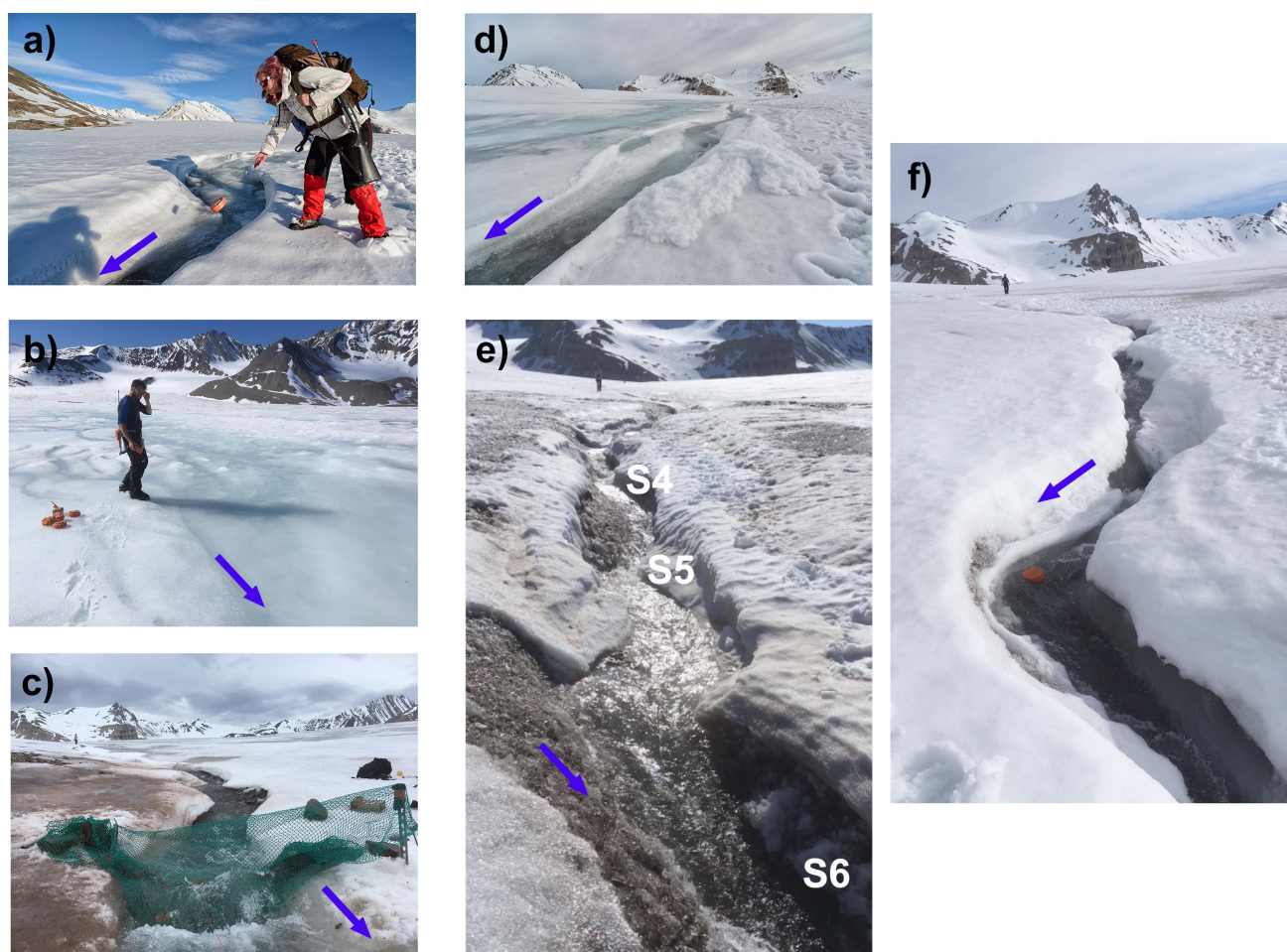


Fig. 3. Pictures from the field deployments. Blue arrows mark the flow direction. a) Deployment point on 30.06.2019 b) Deployment point on 04.07.2019 c) Recovery point on 02.07.2019 d) Slush flows in the upper part of the supraglacial channel on 02.07.2019 e) Lower part of the channel on 04.07.2019 with step-pool sequences S4-6. F) Lower part of the channel on 30.06.2019.

137 Once downsampled, the coordinates were converted to a channel-fitted coordinate system (Legleiter and
138 Kyriakidis, 2006; Tuhtan and others, 2020). The along stream coordinates were then aligned using Dynamic
139 Time Warping Barycenter Averaging (DBA) (Petitjean and others, 2011, 2014; Forestier and others, 2017)
140 for each deployment date (30.06: n=23, 02.07: n=26, 04.07: n=13). The path matrix of the DBA alignment
141 was exported separately.

142 The IMU data was converted to the Earth reference frame and then aligned using the path matrix of the
143 DBA alignment of the along stream coordinates. Velocities were aligned similarly, using the path matrix
144 as well. In a final step, mean values and 95% confidence intervals (CI) were calculated for each day based
145 on the aligned datasets and the data smoothed using moving mean filters (2.4s window length). The whole
146 processing workflow is also shown in figure 4.

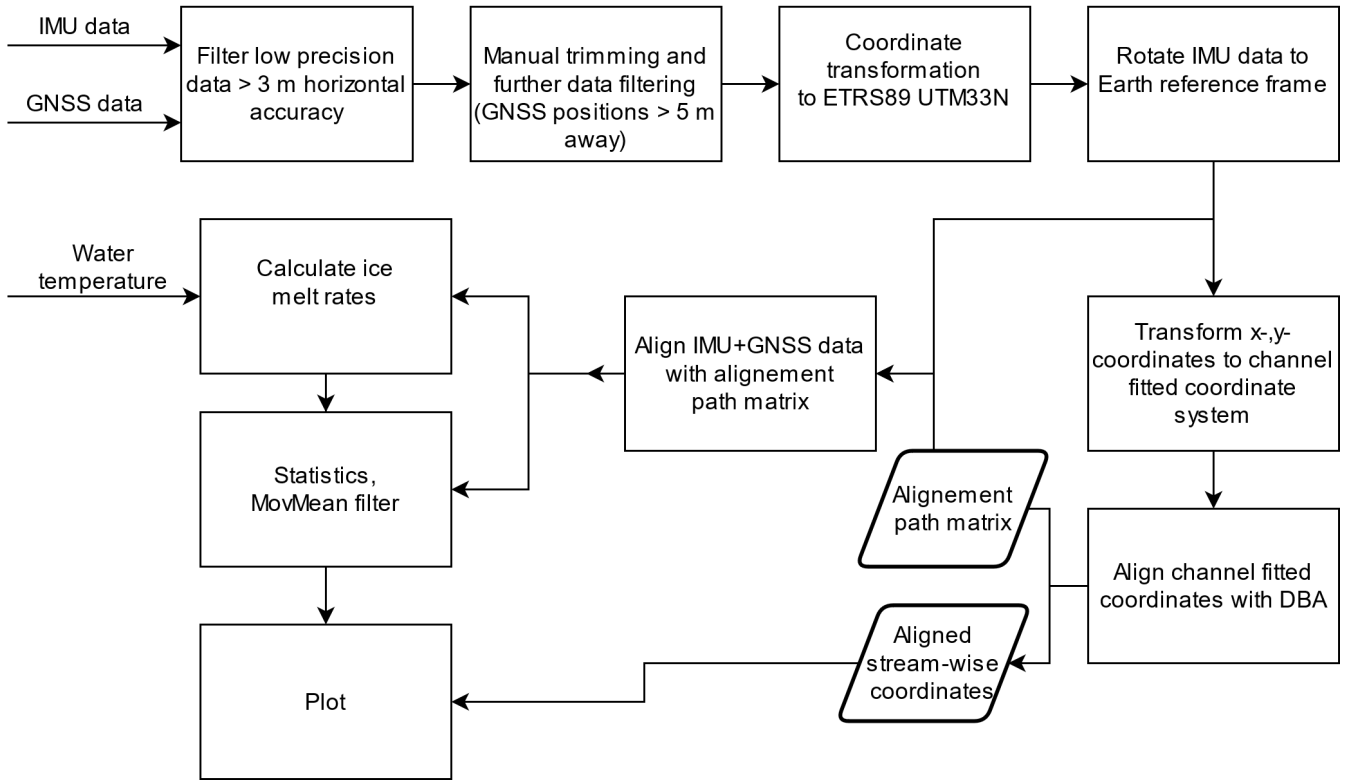


Fig. 4. Overview of the data processing workflow.

147 Calculation of ice melt rates

148 Following Isenko and others (2005) we calculated the ice melt rates along the supraglacial channel:

$$\frac{dr}{dt} = 1.24 \frac{Bv}{q\rho_i} \Delta T \quad (1)$$

149 with r being the radius of a semi-circular channel cross-section, $\frac{dr}{dt}$ being the ice melt rate for an open flow
 150 channel, B a parameter for turbulent flow at 0°C , v the water velocity along the channel, q the latent heat
 151 of melting for ice, ρ_i the density of ice and ΔT the temperature difference between the ice temperature at
 152 the channel walls and the water. We assumed the recorded velocities of the drifters to equal the actual water
 153 velocities v . It is, however, likely that the real water velocities might have been higher, than the obtained
 154 velocities from the drifters. The water temperature was recorded with a HOBO water level logger inside the
 155 supraglacial channel. The recorded temperature of -0.1°C seemed, however, unlikely under atmospheric
 156 conditions. A second HOBO water level logger was located further downstream (orange circle in fig. 2c).
 157 This logger recorded a constant water temperature of 0.01°C . Both recorded values were, however, exposed
 158 to a high uncertainty rating of the temperature sensor of $\pm 0.44^\circ\text{C}$. We therefore assumed a constant water
 159 temperature of 0.01°C , which is a likely value for freshly produced meltwater with ice pieces still inside. We

Table 1. Used parameters and numerical values for the calculation of the ice melt rate along the channel following Isenko and others (2005)

Parameter	Value
Ice density	$\rho_i = 900 \text{ kg m}^{-3}$
Latent heat of melting	$q = 3.35 \times 10^5 \text{ J kg}^{-1}$
Factor for turbulent flow at 0 °C	$B = 2.64 \times 10^3 \text{ J m}^{-3} \text{ K}^{-1}$
Temperature difference	$\Delta T = 0.01 \text{ °C}$
Velocity	<i>Measured</i>

160 further assumed the ice at the channels walls to be at the pressure melting point, resulting in an assumed
161 constant temperature difference of 0.01 °C. The other used numerical values necessary for equation 1 can
162 be found in table 1.

163 MARKOV CHAIN - MONTE CARLO ANALYSIS OF DISCHARGE

164 Markov Chain - Monte Carlo (MCMC) analysis was used to estimate the discharge in the channel. For this
165 we calculated the cross-sectional flow area following the equation from Neal and others (2015):

$$A = wd \left(1 - \frac{1}{s+1} \right), \quad (2)$$

166 where w is the channel width ($2r$ in case of a semi-circular cross-section), d the water depth in the channel
167 and s a geometry factor accounting for the cross-sectional shape of the channel. This geometry factor can
168 take any value larger than 0. A value of $s = 1$ will produce a triangle, $s = 2$ a parabolic channel and larger
169 values of s will result in concave channels and for $s \rightarrow \infty$, it describes a rectangular cross-section Neal and
170 others (2015). We choose a mean value of $s = 6$ (table 2) as this geometry was most representative for the
171 channel cross-sections encountered in the field. Once the cross-sectional flow area is known, the discharge
172 Q can be derived from

$$Q = Av, \quad (3)$$

173 where v is the cross-sectional mean water velocity. For the mean water velocities, the average and standard
174 deviation of the drifter recorded velocities of the last 226 m of the channel were calculated for each day. As
175 none of the other required parameters were measured in the field, we estimated them from pictures and
176 videos taken during the fieldwork. Estimated mean and standard deviations have been used in a Monte
177 Carlo scheme (n=100 000) to assess the related uncertainty range (table 2).

Table 2. Used parameters and statistical distribution for the MCMC analysis with 100 000 runs. The given parameters are all estimated based on field pictures and videos. A Gaussian distribution is assumed for all values

Parameter	Mean value	Standard deviation
Channel width w	0.4 m	0.1 m
Channel depth d	0.1 m	0.03 m
Geometry factor s	6	2
Velocity v	<i>Measured</i>	<i>Measured</i>

178 RESULTS

179 Hydro-meteorological conditions

180 Figure 5 shows the hydro-meteorological conditions during the study period, starting with the
181 measurements in the evening on the 30th of June when the HOBO water level logger was installed in
182 the supraglacial channel. The temperature data recorded at the Ny-Ålesund weather station (available via
183 the Norwegian meteorological service) show peak temperatures between 1st and 2nd of July. This has led
184 to the initiation of the main snow melt in 2019. High discharge in the proglacial river inhibited access to
185 the study site on the 1st of July. The use of the fishing net for drifter recovery led to water damming due
186 to ice accumulation in the net. This damming resulted in a water level drop downstream of the net, where
187 the stage gauge was located (fig. 5b). Another discharge peak, due to spiking air temperatures, took place
188 on the last study day on the 4th of July.

189 Velocities

190 Our results show velocities between 1 and 3 m s⁻¹ with the highest velocities at the lower section of the
191 channel (fig. 6-9). Statistical analysis of the last 226 m of the channel section, measured on all three field
192 days, resulted in mean values of 1.94 m s⁻¹ (30.06), 2.14 m s⁻¹ (02.07) and 1.85 m s⁻¹ (04.07). The standard
193 deviations were 0.32 m s⁻¹ (30.06), 0.50 m s⁻¹ (02.07) and 0.26 m s⁻¹ (04.07). All values are also shown in
194 table 3. This shows an increase of velocities with increasing air temperature (discharge). The velocities
195 are generally not evenly distributed along the channel but rather follow prominent shapes (fig. 6-9), which
196 can be related to the morphology of the channel with peak velocities around meander bends and step-pool
197 sequences. These shapes become also more pronounced with increasing discharge (visible in the higher
198 standard deviation).



Fig. 5. Hydro-meteorological conditions during the study period. A) Recorded air temperature in Ny-Ålesund. B) Recorded water pressure and water temperature in the studied supraglacial channel.

199 Accelerations

200 Acceleration magnitudes are mostly between 3 and 7 m s^{-2} along the flow path with peaks up to 8 m s^{-2}
 201 (fig. 6-9). Clearly visible peaks in the lower section of the channel are related to step-pool sequences (fig.
 202 6-9), where the maximum acceleration occurs at the edge of the step in a step-pool sequence (Alexander
 203 and others, 2020a). The mean values of the acceleration magnitude (see table 3) show a trend towards
 204 higher accelerations as the channel develops and the morphological features, such as step-pool sequences,
 205 meanders and chutes, become more pronounced.

206 Ice melt rates

207 Ice melt rates are calculated, assuming water temperature of 0.01 °C. The resulting ice melt rates follow
 208 the same distribution as the velocities (fig. 9), due to the direct proportionality in equation 1. The derived

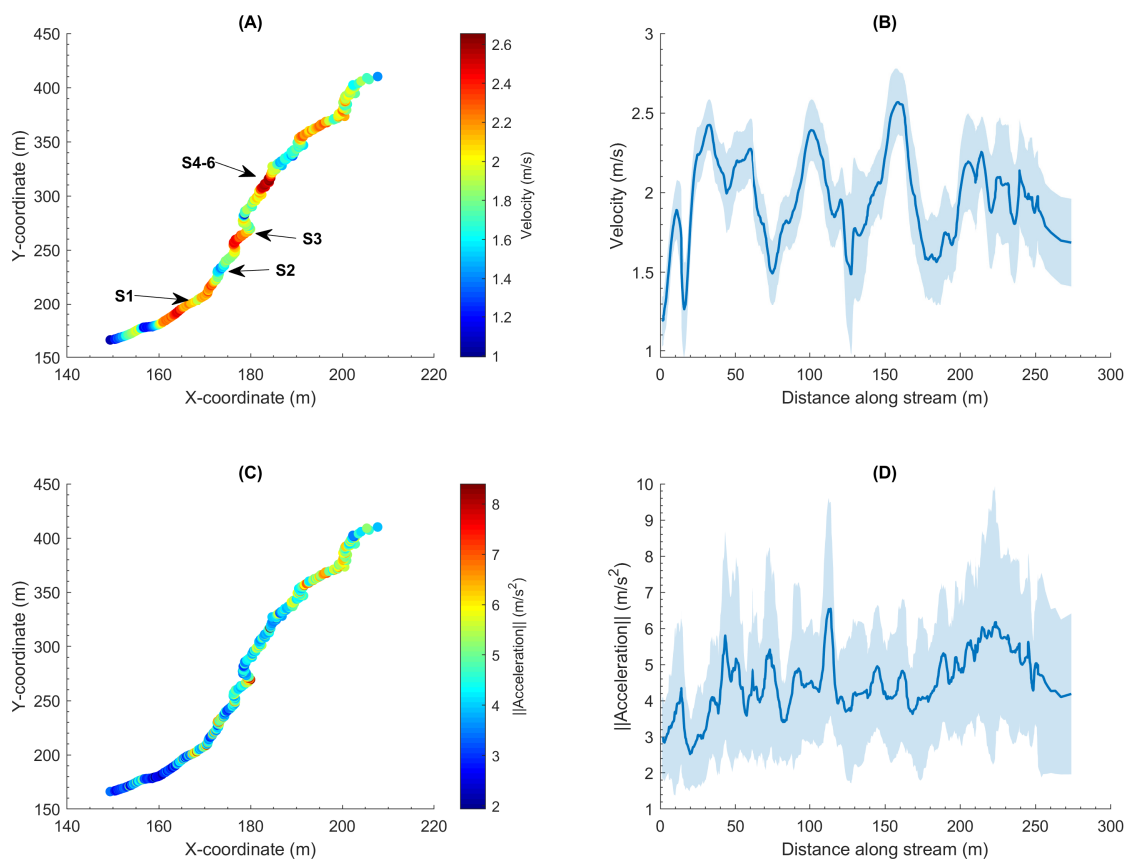


Fig. 6. Channel geometry with velocities and accelerations on 30.06.2019 ($n=23$). All data is plotted using a 2.4 s MovMean filter. A) Local coordinate system (based on the deployment point on 4th of July) with recorded velocities. The locations of step-pool sequences S1-S6 are indicated on the map as well. B) Mean velocity distribution along the channel transect with 95% confidence interval (CI). C) Local coordinate system with recorded absolute acceleration mean values. D) Mean absolute acceleration distribution along the channel transect with 95% CI.

209 ice melt rates are mostly in the range between 1 and 3 cm per day. The highest ice melt rates occur around
 210 step-pool sequences and shortly before the turn at meander bends. The ice melt rates increase with the
 211 discharge and as such vary greatly over time and space (see table 3).

212 Discharge

213 The calculated discharge of $0.06 \text{ m}^3 \text{ s}^{-1}$ (30.06 and 04.07) and $0.07 \text{ m}^3 \text{ s}^{-1}$ (02.07) is rather low (fig. 10),
 214 being in good accordance with the small size of the investigated channel. The simulations have, however,
 215 very high uncertainties resulting from the estimation of the input parameters. The uncertainty, given in
 216 the 95% CI (see table 3), can reach up to $\pm 50\%$ of the simulated mean value for the discharge.

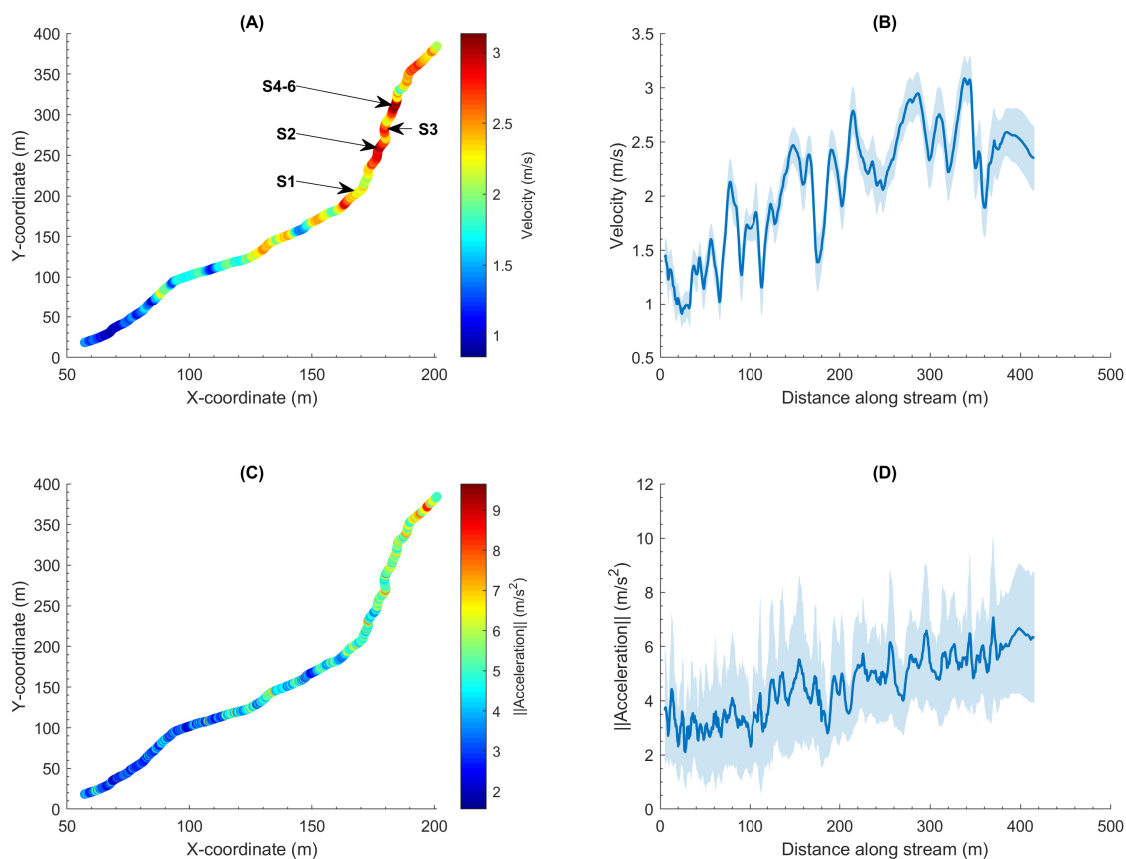


Fig. 7. Channel geometry with velocities and accelerations on 02.07.2019 (n=26). All data is plotted using a 2.4 s MovMean filter. A) Local coordinate system (based on the deployment point on 4th of July) with recorded velocities. The locations of step-pool sequences S1-S6 are indicated on the map as well. B) Mean velocity distribution along the channel transect with 95% confidence interval (CI). C) Local coordinate system with recorded absolute acceleration mean values. D) Mean absolute acceleration distribution along the channel transect with 95% CI.

Table 3. Mean values and standard deviations (std) of velocity, absolute acceleration and computed ice melt rate for the last 226 m of the channel for all three field days: 30.06.2019 (n=23), 02.07.2019 (n=26) and 04.07.2019 (n=13). Additionally reported are the mean discharge values of the MCMC analysis (n=100 000) with 95% CI

Parameter	30.06		02.07		04.07	
	Mean	Std	Mean	Std	Mean	Std
Velocity (m s^{-1})	1.94	0.32	2.14	0.50	1.85	0.26
Acceleration (m s^{-2})	4.43	1.12	4.61	1.28	4.84	1.24
Ice melt rate (cm d^{-1})	1.82	0.30	2.01	0.47	1.74	0.24
Discharge ($\text{m}^3 \text{s}^{-1}$)	0.06	0.04-0.09 CI	0.07	0.04-0.10 CI	0.06	0.04-0.09 CI

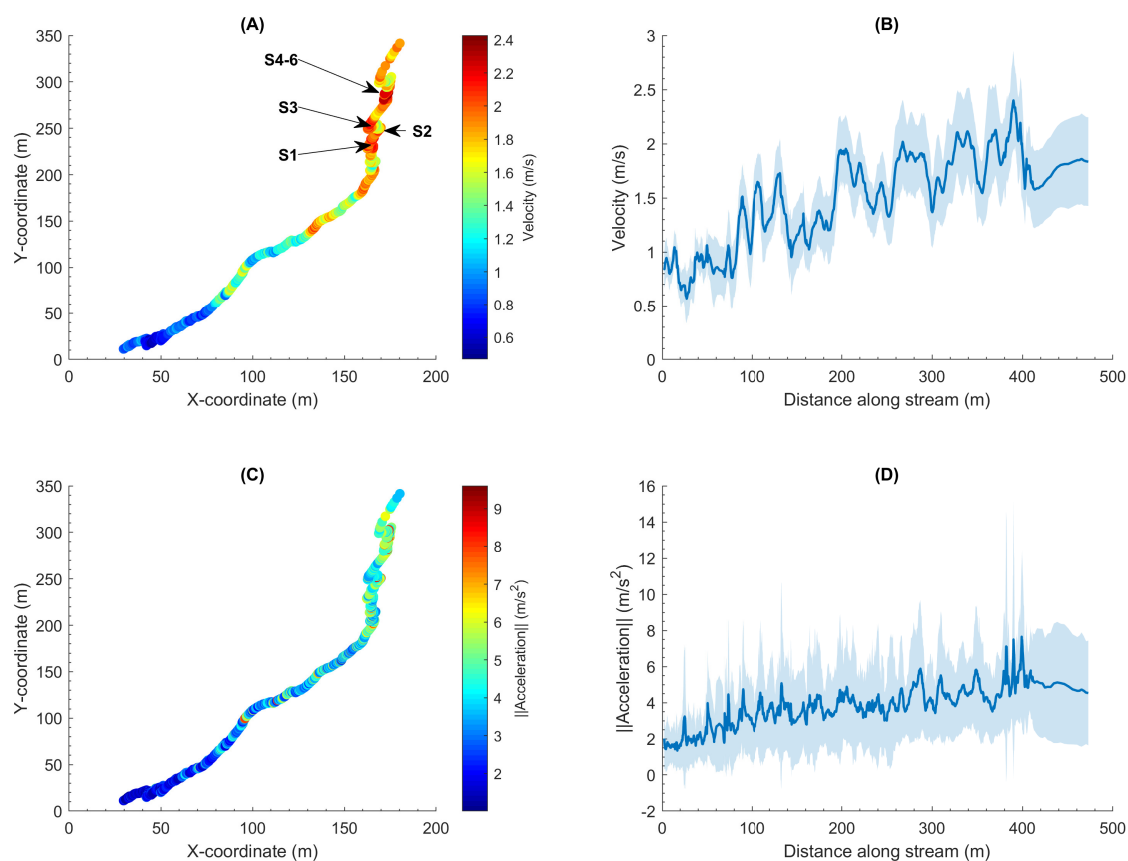


Fig. 8. Channel geometry with velocities and accelerations on 04.07.2019 ($n=13$). All data is plotted using a 2.4 s MovMean filter. A) Local coordinate system (based on the deployment point on 4th of July) with recorded velocities. The locations of step-pool sequences S1-S6 are indicated on the map as well. B) Mean velocity distribution along the channel transect with 95% confidence interval (CI). C) Local coordinate system with recorded absolute acceleration mean values. D) Mean absolute acceleration distribution along the channel transect with 95% CI.

217 DISCUSSION

218 Using GNSS enabled surface drifters allows to quickly map hydraulic variables along supraglacial channels,
 219 thereby having a clear advantage over point measurements or approaches that provide spatially-integrated
 220 information, such as dye tracing. The drifters capture the spatial distribution of velocities, revealing a more
 221 diverse picture than it is possible with point measurements. Compared to spatially-integrating approaches
 222 (e.g. dye-tracing) a lot more information can be obtained. In comparison to mean values, which could also
 223 be obtained using with dye-tracing, local velocities can be up to 50% higher. This is of relevance when
 224 considering ice melt rates and trying to model the evolution of the supraglacial channel towards en- and
 225 subglacial drainage systems. An approach based on mean velocities, as obtained by dye-tracing, would

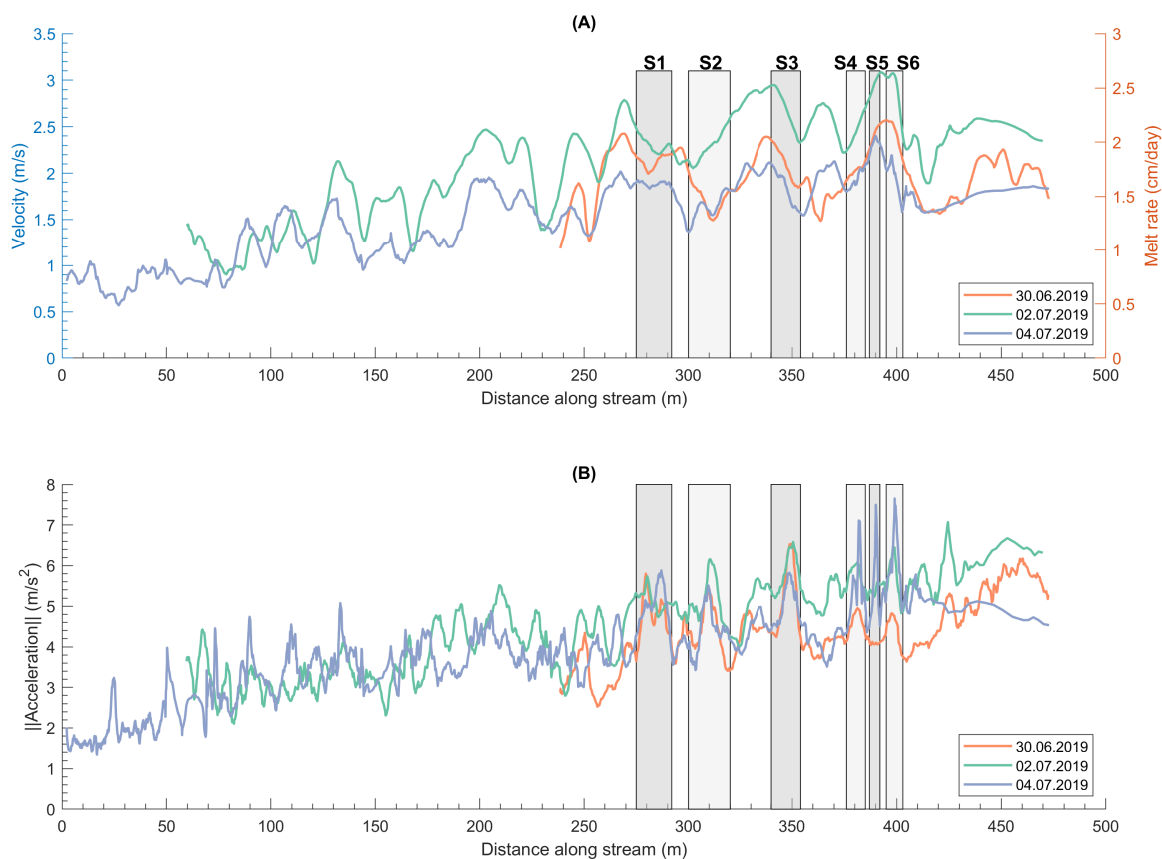


Fig. 9. Mean values of velocity, absolute acceleration and calculated ice melt rate along the channel transects compared for the study period. All data are plotted using a 2.4 s MovMean filter. A) Recorded mean velocities on 30.06.2019 (n=23), 02.07.2019 (n=26) and 04.07.2019 (n=13) along the channel transect with step-pool sequences S1-S6 marked with grey boxes. Further shown is the derived ice melt rate along the transect. B) Recorded absolute mean accelerations along the channel transect.

226 lead to a uniform incision rate of the channel and result in a poor representation of reality.

227

228 The calculation of ice melt rates, based on drifter derived velocities, shows good accordance with field
 229 measurements from other studies that were between 2 and 5.8 cm d⁻¹ (e.g. Marston, 1983). McGrath and
 230 others (2011) additionally reported some more recent measurements from a small supraglacial channel
 231 on the GrIS. The mean incision rate was thereby 3.30 ± 0.47 cm d⁻¹ (McGrath and others, 2011). Our
 232 computed ice melt rates are non-uniformly distributed along the channel with the highest values in the
 233 lower section of the channel around meander bends, chutes and step-pool sequences, where the surface
 234 slope and therefore the water velocities are highest. This follows the direct proportionality between ice melt

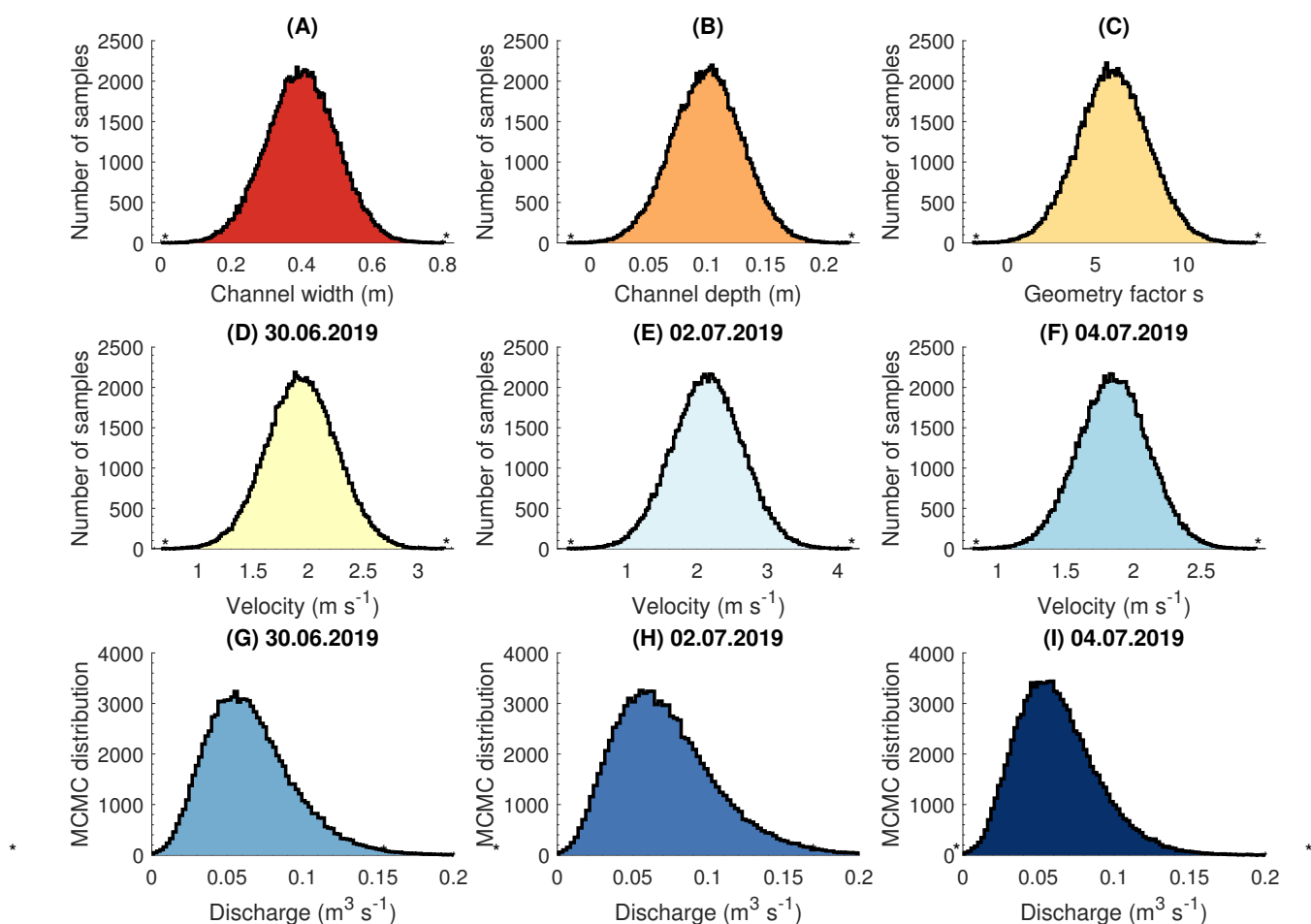


Fig. 10. MCMC analysis ($n=100\,000$) to obtain the discharge on the three observation days. Gaussian distribution of A) the estimated channel width, B) the estimated channel depth and C) the estimated geometry factor s . The measured average velocity with standard deviation of the last 226 m served as base to assess the combined uncertainty: D) velocity distribution on 30.06.2019, E) velocity distribution on 02.07.2019 and F) velocity distribution on 04.07.2019. Resulting statistical distributions for the derived discharge: G) 30.06.2019, H) 02.07.2019 and I) 04.07.2019.

235 rate and velocity from equation 1. Expectedly, ice melt rates also increase over time as the discharge goes up.

236

237 However, our zones of highest ice melt rates do not match the zones, where the highest melt rates would
 238 be expected following other field studies. Both Vatne and Irvine-Fynn (2016) and Kamintzis and others
 239 (2019) show that the highest ice melt rates occur at the bottom of step-risers, before the plunge pool
 240 begins. Our results likely do not match these observations as we only take kinetic energy into account, by
 241 keeping the water temperature constant. In the case of step-pool sequences, additional potential energy
 242 dissipation needs to be considered. The potential energy is dissipated by increasing the water temperature,

243 followed by the rapid return to the equilibrium temperature within the plunge pool (Isenko and others,
244 2005). Secondary circulation (Venditti and others, 2014) at the end of the plunge pool further reduces
245 the heat energy rapidly (Vatne and Irvine-Fynn, 2016). This in turn leads to additional high ice melt
246 rate within the plunge pool and is not taken into account by our velocity based approach as we keep the
247 water temperature at a constant level. It needs to be further emphasized that our derived ice melt rates
248 are exposed to high uncertainty. We have assumed a constant temperature difference of 0.01 °C between
249 ice and water. We have, however, not measured the ice temperature in the field and the measured water
250 temperature is outside the accuracy rating of the used water level logger, leading to a high expected
251 uncertainty. Utilizing the expected temperature for ice water, the uncertainty can, however, be reduced.
252 An accurate mapping of the spatial ice melt rate distribution along supraglacial channels with drifters will,
253 however, require additional temperature sensing capabilities, as well as further field studies to validate the
254 calculations with field measurements of actually occurring ice melt rates.

255

256 The calculated discharge is with mean values of $0.06\text{ m}^3\text{ s}^{-1}$ to $0.07\text{ m}^3\text{ s}^{-1}$ in a good accordance
257 with other discharge values reported for smaller streams in the scientific literature. Gleason and
258 others (2016) reported $0.006\text{ m}^3\text{ s}^{-1}$ to $0.402\text{ m}^3\text{ s}^{-1}$ for small streams on the GrIS, Marston (1983)
259 measured $0.04\text{ m}^3\text{ s}^{-1}$ to $0.20\text{ m}^3\text{ s}^{-1}$ on the Juneau Icefield (Alaska), Schuler and others (2004) reported
260 $0.05\text{ m}^3\text{ s}^{-1}$ to $0.4\text{ m}^3\text{ s}^{-1}$ at Unteraargletscher (Swiss Alps) and McGrath and others (2011) showed
261 discharge values of $0.017\text{ m}^3\text{ s}^{-1}$ to $0.54\text{ m}^3\text{ s}^{-1}$ for a small supraglacial stream feeding into a moulin
262 on the GrIS. The uncertainties of our method are, however, very high and can account for up to 50%
263 of the estimated value. This shows that our approach can be used to obtain a first estimate of the
264 discharge, especially in cases where available field measurements are limited. A more precise estimation
265 will, however, need further constraints of the input parameters. This could for example be done with
266 remote sensing derived measurements of channel width and water depth in case of larger supraglacial rivers.

267

268 Mapping of the accelerations confirms the observations already made by Alexander and others (2020a).
269 Clear and pronounced signal peaks in the acceleration data mark the occurrence of meander-bends and
270 step-pools sequences with the latter being pronounced more clearly. Further on, table 3 shows that the
271 water accelerations increase, as the channel develops. The accelerations are thereby increasing despite
272 decreasing discharge. We explain this by the morphological development of the channel towards higher

273 accelerations and decelerations of the water with more pronounced morphology. At the start of the field
274 experiment, the channel was not fully developed yet. Over the preceding days the channel was cleared
275 from any remaining slush and the high discharge during the peak melt period (1st and 2nd of July) led
276 to high velocities. This resulted in high ice melt rates and therefore the morphological development of
277 the channel. As a result, the water was accelerated and decelerated more and the absolute acceleration
278 of the water increased, mainly due to the development of more pronounced meander bends and step-
279 pool sequences. We speculate that this trend of increasing water accelerations continues throughout the
280 melt-season, topping towards the late-melt season, shortly before the discharge finally drops to lower levels.

281

282 At the start of the fieldwork (30.06) only three step-pool sequences existed in the lower section of
283 the channel (last 226 m). These were S1, S3, and S6. Two days later on the 2nd of July two additional
284 step-pool sequences had developed (S2, S4), followed by the development of S5 by the 4th of July. Even
285 though the step-pool sequences were not visually detectable in the channel on the first day of the fieldwork,
286 their signature can already be seen in the acceleration records (fig. 9). With exception for S5, all other
287 step-pool sequences show already clear and pronounced peaks in the acceleration data on the 30th of June.
288 We therefore suggest that accelerations can be used to predict the morphological evolution of supraglacial
289 channels. Zones of abrupt and rapid changes in acceleration, will lead to rapid changes in velocity and
290 hence also ice melt. This results in enhanced melt around zones of abrupt and large acceleration changes
291 and thus the development of pronounced channel morphology. This is also in agreement with observations
292 made by Germain and Moorman (2016). They showed that the development of step-pool sequences is not
293 necessarily linked to high discharge but might as well be connected to the location of transverse fractures
294 in the channel (Germain and Moorman, 2019). Similar to their observations, we observe the formation
295 of step-pool sequences during dropping discharge. We did not investigate for fractures in the channel
296 during the fieldwork but the existence of structural features within the channel might, however, lead
297 to disturbances of the flow and hence increased acceleration, followed by the development of step-pool
298 sequences. The observation of spatio-temporal acceleration distributions will therefore give valuable insight
299 into channel evolution and should receive more attention in future hydrological studies.

300

301 A focus on accelerations would also open up new opportunities to validate hydrological models that
302 simulate the evolution of channels. We are convinced that acceleration records can be used to detect

303 channel morphologies in cases where a visual control is not possible (e.g. en- and subglacial channels).
304 Further planned field studies will therefore focus on gathering channel morphology measurements to link
305 these to the obtained drifter records. Furthermore, dye-tracer experiments should be conducted in parallel
306 to drifter deployments to better compare drifter based results and classical dye-tracing studies. This will
307 also be necessary in order to elucidate the degree to which GNSS derived drifter velocities represent the
308 actual water velocity. Having clarified these questions, our drifter based approach will allow for novel
309 field-based studies that can provide valuable and extensive insight into the spatial and temporal evolution
310 of supraglacial streams.

311

312 CONCLUSIONS

313 We have conducted studies with GNSS enabled drifters at a small supraglacial channel on Austre
314 Brøggerbreen (Svalbard). Our drifters allow for measurements of spatially referenced channel flow paths,
315 water velocities and accelerations. By estimating water temperatures, ice melt rates along the channel can
316 be derived. MCMC analysis allows to further estimate the discharge in the channel. Our measurements
317 show high variability in space and time with most pronounced characteristics in areas of meander bends and
318 step-pool sequences. Local water velocities can be up to 50% higher, compared to mean values, showing
319 the importance of spatial measurements for correct channel incision modeling. Derived ice melt rates
320 are with 1 cm d^{-1} to 3 cm d^{-1} in good accordance with published values of similar sized channels (e.g.
321 Marston, 1983; McGrath and others, 2011). The discharge in the channel is estimated to $0.06 \text{ m}^3 \text{ s}^{-1}$ to
322 $0.07 \text{ m}^3 \text{ s}^{-1}$, has, however, high uncertainty of up to 50% due to lacking field based parameter constriction.
323 Several step-pool sequences developed in the channel during dropping discharge, leading to increasing
324 acceleration magnitudes. The location of the step-pool sequence development could already be predicted
325 beforehand from the acceleration records by clearly pronounced signal peaks. We therefore conclude that
326 water acceleration can be used to predict where step-pool sequences will form. Acceleration measurements
327 further allow to identify morphological features within the channel, which will be of relevance when
328 investigating subsurface or deeply incised channels. Future field investigations of supraglacial streams and
329 rivers should therefore also gather information on accelerations to further investigate channel evolution.

330 AUTHOR CONTRIBUTIONS

331 AA designed the study, processed all data and prepared the manuscript. AA, JAT and MK conducted the
332 fieldwork. All authors contributed to the interpretation of the results and the manuscript.

333 ACKNOWLEDGEMENTS

334 The fieldwork for this project was funded by the INTERACT Transnational Access project DeepSense 2019,
335 University of Oslo Industrial Liason, University of Oslo Garpen Stipend, the Department of Geosciences
336 University of Oslo, the Research Council of Norway funded MAMMAMIA project (NFR: 301837,
337 MAMMAMIA: Multi-scale multi-method analysis of mechanisms causing ice acceleration) and the Svalbard
338 Environmental protection fund (17/31). AA acknowledges partial funding from the European Research
339 Council grant ICEMASS. This study is a contribution to the Svalbard Integrated Earth Observatory
340 (SIOS). We further on acknowledge support from the team of the NPI Sverdrup station, particularly Vera
341 Sklet, during the fieldwork.

342 REFERENCES

- 343 Alexander A, Kruusmaa M, Tuhtan JA, Hodson AJ, Schuler TV and Kääh A (2020a) Pressure and inertia sensing
344 drifters for glacial hydrology flow path measurements. *The Cryosphere*, **14**(3), 1009–1023, ISSN 1994-0416 (doi:
345 <https://doi.org/10.5194/tc-14-1009-2020>), publisher: Copernicus GmbH
- 346 Alexander A, Obu J, Schuler TV, Kääh A and Christiansen HH (2020b) Subglacial permafrost dynamics and erosion
347 inside subglacial channels driven by surface events in svalbard. *The Cryosphere*, **14**(11), 4217–4231 (doi: 10.5194/tc-
348 14-4217-2020)
- 349 Barrand NE, James TD and Murray T (2010) Spatio-temporal variability in elevation changes of two high-arctic
350 valley glaciers. *Journal of Glaciology*, **56**(199), 771–780 (doi: 10.3189/002214310794457362)
- 351 Behrens T, Schmidt K, MacMillan R and Rossel RV (2018) Multiscale contextual spatial modelling with the gaussian
352 scale space. *Geoderma*, **310**, 128–137
- 353 Boulton GS and Hindmarsh RCA (1987) Sediment deformation beneath glaciers: Rheology and geological
354 consequences. *Journal of Geophysical Research: Solid Earth*, **92**(B9), 9059–9082, ISSN 2156-2202 (doi:
355 10.1029/JB092iB09p09059), eprint: <https://agupubs.onlinelibrary.wiley.com/doi/pdf/10.1029/JB092iB09p09059>
- 356 Decaux L, Grabiec M, Ignatiuk D and Jania J (2019) Role of discrete water recharge from supraglacial drainage
357 systems in modeling patterns of subglacial conduits in Svalbard glaciers. *The Cryosphere*, **13**(3), 735–752, ISSN
358 1994-0416 (doi: <https://doi.org/10.5194/tc-13-735-2019>)

- 359 Dunse T, Schellenberger T, Hagen JO, Kääb A, Schuler TV and Reijmer CH (2015) Glacier-surge mechanisms
360 promoted by a hydro-thermodynamic feedback to summer melt. *The Cryosphere*, **9**(1), 197–215
- 361 Forestier G, Petitjean F, Dau HA, Webb GI and Keogh E (2017) Generating synthetic time series to augment sparse
362 datasets. In *Data Mining (ICDM), 2017 IEEE International Conference on*, 865–870, IEEE
- 363 Germain SLS and Moorman BJ (2016) The development of a pulsating supraglacial stream. *Annals of Glaciology*,
364 **57**(72), 31–38, ISSN 0260-3055, 1727-5644 (doi: 10.1017/aog.2016.16)
- 365 Germain SLS and Moorman BJ (2019) Long-term observations of supraglacial streams on an Arctic glacier. *Journal*
366 *of Glaciology*, 1–12, ISSN 0022-1430, 1727-5652 (doi: 10.1017/jog.2019.60)
- 367 Gleason CJ and 8 others (2016) Characterizing supraglacial meltwater channel hydraulics on the Greenland Ice
368 Sheet from in situ observations. *Earth Surface Processes and Landforms*, **41**(14), 2111–2122, ISSN 1096-9837 (doi:
369 10.1002/esp.3977)
- 370 Gulley J, Benn D, Müller D and Luckman A (2009) A cut-and-closure origin for englacial conduits in uncrevassed
371 regions of polythermal glaciers. *Journal of Glaciology*, **55**(189), 66–80, ISSN 0022-1430, 1727-5652 (doi:
372 10.3189/002214309788608930)
- 373 Hagen J, Korsen O and Vatne G (1991) Drainage pattern in a subpolar glacier: Brøggerbreen, svalbard. *Arctic*
374 *Hydrology, Present and Future Tasks*, 121–131
- 375 Hanssen-Bauer I, Førland E, Hisdal H, Mayer S, Sandø A and Sorteberg A (eds.) (2019) *Climate in Svalbard 2100–a*
376 *knowledge base for climate adaptation*, volume 1. Norsk klimaservicesenter (NKSS)/Norwegian Centre for Climate
377 Services (NCCS)
- 378 Iken A and Bindschadler RA (1986) Combined measurements of Subglacial Water Pressure and Surface Velocity of
379 Findelengletscher, Switzerland: Conclusions about Drainage System and Sliding Mechanism. *Journal of Glaciology*,
380 **32**(110), 101–119, ISSN 0022-1430, 1727-5652 (doi: 10.3189/S0022143000006936)
- 381 Isenko E, Naruse R and Mavlyudov B (2005) Water temperature in englacial and supraglacial channels: Change
382 along the flow and contribution to ice melting on the channel wall. *Cold Regions Science and Technology*, **42**(1),
383 53–62, ISSN 0165-232X (doi: 10.1016/j.coldregions.2004.12.003)
- 384 Jarosch AH and Gudmundsson MT (2012) A numerical model for meltwater channel evolution in glaciers. *The*
385 *Cryosphere*, **6**(2), 493–503, ISSN 1994-0424 (doi: 10.5194/tc-6-493-2012)
- 386 Kääb A, Altena B and Mascaro J (2019) River-ice and water velocities using the planet optical cubesat constellation.
387 *Hydrology and Earth System Sciences*, **23**(10), 4233–4247 (doi: 10.5194/hess-23-4233-2019)
- 388 Kamintzis JE and 6 others (2019) Knickpoint evolution in a supraglacial stream. *Geografiska Annaler: Series A*,
389 *Physical Geography*, **101**(2), 118–135, publisher: Taylor & Francis
- 390 Karlstrom L, Gajjar P and Manga M (2013) Meander formation in supraglacial streams. *Journal of Geophysical*
391 *Research: Earth Surface*, **118**(3), 1897–1907, ISSN 2169-9011 (doi: 10.1002/jgrf.20135)

- 392 Legleiter CJ and Kyriakidis PC (2006) Forward and inverse transformations between cartesian and channel-fitted
393 coordinate systems for meandering rivers. *Mathematical Geology*, **38**(8), 927–958
- 394 Legleiter CJ, Tedesco M, Smith LC, Behar AE and Overstreet BT (2014) Mapping the bathymetry of supraglacial
395 lakes and streams on the Greenland Ice Sheet using field measurements and high resolution satellite images. **8**(1),
396 215–228 (doi: 10.7916/D87W6C3B)
- 397 Mair D, Nienow P, Sharp M, Wohlleben T and Willis I (2002) Influence of subglacial drainage system
398 evolution on glacier surface motion: Haut Glacier d’Arolla, Switzerland. *Journal of Geophysical Research: Solid*
399 *Earth*, **107**(B8), EPM 8–1–EPM 8–13, ISSN 2156-2202 (doi: <https://doi.org/10.1029/2001JB000514>), eprint:
400 <https://agupubs.onlinelibrary.wiley.com/doi/pdf/10.1029/2001JB000514>
- 401 Mantelli E, Camporeale C and Ridolfi L (2015) Supraglacial channel inception: Modeling and processes. *Water*
402 *Resources Research*, **51**(9), 7044–7063, ISSN 0043-1397 (doi: 10.1002/2015WR017075)
- 403 Marston RA (1983) Supraglacial Stream Dynamics on the Juneau Icefield. *Annals of the Association of American*
404 *Geographers*, **73**(4), 597–608, ISSN 0004-5608, 1467-8306 (doi: 10.1111/j.1467-8306.1983.tb01861.x)
- 405 McGrath D, Colgan W, Steffen K, Lauffenburger P and Balog J (2011) Assessing the summer water budget of a
406 moulin basin in the Sermeq Avannarleq ablation region, Greenland ice sheet. *Journal of Glaciology*, **57**(205),
407 954–964, ISSN 0022-1430, 1727-5652 (doi: 10.3189/002214311798043735)
- 408 Neal JC and 7 others (2015) Efficient incorporation of channel cross-section geometry uncertainty into regional
409 and global scale flood inundation models. *Journal of Hydrology*, **529**, 169–183, ISSN 0022-1694 (doi:
410 10.1016/j.jhydrol.2015.07.026)
- 411 Nienow PW, Sole AJ, Slater DA and Cowton TR (2017) Recent Advances in Our Understanding of the Role of
412 Meltwater in the Greenland Ice Sheet System. *Current Climate Change Reports*, **3**(4), 330–344, ISSN 2198-6061
413 (doi: 10.1007/s40641-017-0083-9)
- 414 Nuth C and 7 others (2013) Decadal changes from a multi-temporal glacier inventory of Svalbard. *The Cryosphere*,
415 **7**(5), 1603–1621, ISSN 1994-0416 (doi: <https://doi.org/10.5194/tc-7-1603-2013>), publisher: Copernicus GmbH
- 416 Petitjean F, Ketterlin A and Gançarski P (2011) A global averaging method for dynamic time warping, with
417 applications to clustering. *Pattern Recognition*, **44**(3), 678–693
- 418 Petitjean F, Forestier G, Webb GI, Nicholson AE, Chen Y and Keogh E (2014) Dynamic time warping averaging
419 of time series allows faster and more accurate classification. In *Data Mining (ICDM), 2014 IEEE International*
420 *Conference on*, 470–479, IEEE
- 421 Phillips T, Rajaram H and Steffen K (2010) Cryo-hydrologic warming: A potential mechanism for rapid thermal
422 response of ice sheets. *Geophysical Research Letters*, **37**(20)

- 423 Phillips T, Rajaram H, Colgan W, Steffen K and Abdalati W (2013) Evaluation of cryo-hydrologic warming as an
424 explanation for increased ice velocities in the wet snow zone, Sermeq Avannarleq, West Greenland. *Journal of*
425 *Geophysical Research: Earth Surface*, **118**(3), 1241–1256
- 426 Pitcher LH and Smith LC (2019) Supraglacial Streams and Rivers. *Annual Review of Earth and Planetary*
427 *Sciences*, **47**(1), 421–452 (doi: 10.1146/annurev-earth-053018-060212), eprint: [https://doi.org/10.1146/annurev-](https://doi.org/10.1146/annurev-earth-053018-060212)
428 [earth-053018-060212](https://doi.org/10.1146/annurev-earth-053018-060212)
- 429 Pope A, Murray T and Luckman A (2007) DEM quality assessment for quantification of glacier surface change. *Annals*
430 *of Glaciology*, **46**, 189–194, ISSN 0260-3055, 1727-5644 (doi: 10.3189/172756407782871792), publisher: Cambridge
431 University Press
- 432 Rippin DM, Pomfret A and King N (2015) High resolution mapping of supra-glacial drainage pathways reveals link
433 between micro-channel drainage density, surface roughness and surface reflectance. *Earth Surface Processes and*
434 *Landforms*, **40**(10), 1279–1290, ISSN 0197-9337 (doi: 10.1002/esp.3719)
- 435 Schuler T, Fischer U and Gudmundsson G (2004) Diurnal variability of subglacial drainage conditions as revealed
436 by tracer experiments. *Journal of Geophysical Research: Earth Surface*, **109**(F2)
- 437 Smith LC and 15 others (2015) Efficient meltwater drainage through supraglacial streams and rivers on the southwest
438 Greenland ice sheet. *Proceedings of the National Academy of Sciences*, **112**(4), 1001–1006, ISSN 0027-8424, 1091-
439 6490 (doi: 10.1073/pnas.1413024112)
- 440 Smith LC and 22 others (2017) Direct measurements of meltwater runoff on the Greenland ice sheet surface.
441 *Proceedings of the National Academy of Sciences*, **114**(50), E10622–E10631, ISSN 0027-8424, 1091-6490 (doi:
442 10.1073/pnas.1707743114)
- 443 Team Planet (2017) Planet application program interface: In space for life on earth
- 444 Tuhtan JA, Kruusmaa M, Alexander A and Fuentes-Pérez J (2020) Multiscale change detection in a supraglacial
445 stream using surface drifters. In *River Flow 2020*, CRC Press (doi: 10.1201/b22619-205)
- 446 Vatne G and Irvine-Fynn TDL (2016) Morphological dynamics of an englacial channel. *Hydrology and Earth System*
447 *Sciences*, **20**(7), 2947–2964, ISSN 1027-5606 (doi: <https://doi.org/10.5194/hess-20-2947-2016>)
- 448 Venditti JG, Rennie CD, Bomhof J, Bradley RW, Little M and Church M (2014) Flow in bedrock canyons. *Nature*,
449 **513**(7519), 534–537
- 450 Willis MJ and 11 others (2018) Massive destabilization of an Arctic ice cap. *Earth and Planetary Science Letters*,
451 **502**, 146–155, ISSN 0012-821X (doi: 10.1016/j.epsl.2018.08.049)
- 452 Yang K, Smith LC, Chu VW, Gleason CJ and Li M (2015) A Caution on the Use of Surface Digital Elevation
453 Models to Simulate Supraglacial Hydrology of the Greenland Ice Sheet. *IEEE Journal of Selected Topics in Applied*
454 *Earth Observations and Remote Sensing*, **8**(11), 5212–5224, ISSN 2151-1535 (doi: 10.1109/JSTARS.2015.2483483),
455 conference Name: IEEE Journal of Selected Topics in Applied Earth Observations and Remote Sensing

456 Yang K and 6 others (2016) Fluvial morphometry of supraglacial river networks on the southwest Greenland Ice
457 Sheet. *GIScience & Remote Sensing*, **53**(4), 459–482, ISSN 1548-1603 (doi: 10.1080/15481603.2016.1162345)